Electronic bandgap miniaturized UWB antenna for near-field microwave investigation of skin

Cite as: AIP Advances **11**, 035228 (2021); https://doi.org/10.1063/5.0030126
Submitted: 19 September 2020 • Accepted: 19 February 2021 • Published Online: 12 March 2021

Sameer Alani, Zahriladha Zakaria, Tale Saeidi, et al.

Electronic bandgap miniaturized UWB antenna for near-field microwave investigation of skin

Cite as: AIP Advances 11, 035228 (2021); doi: 10.1063/5.0030126
Submitted: 19 September 2020 • Accepted: 19 February 2021 •
Published Online: 12 March 2021

Sameer Alani,[1,a)] Zahriladha Zakaria,[2,a)] Tale Saeidi,[3] Asmala Ahmad,[1] Hussein Alsariera,[2] Othman S. Al-Heety,[2] and Sarmad Nozad Mahmood[4]

AFFILIATIONS

[1]Centre for Advanced Computing Technolgy (C-ACT), Faculty of Information and Communication Technology, Universiti Teknikal Malaysia Melaka, Hang Tuah Jaya, 76100 Durian Tunggal, Melaka, Malaysia
[2]Centre for Telecommunication Research and Innovation (CeTRI), Faculty of Electronic and Computer Engineering, Universiti Teknikal Malaysia Melaka (UTeM), 76100 Durian Tunggal, Melaka, Malaysia
[3]Electrical and Electronic Engineering Department of Universiti Teknologi PETRONAS, Bandar Seri Iskandar, 32610 Perak, Malaysia
[4]Department of Electrical and Electronic Engineering, Faculty of Engineering, Universiti Putra Malaysia, Serdang, Selangor 43300, Malaysia

[a)]**Authors to whom correspondence should be addressed:** Sameer@siswa.ukm.edu.my and zahriladha@utem.edu.my

ABSTRACT

Near-field microwave investigation and tomography has many practical applications, especially where the trend of fields and signals in different environments is vital. This article shows an elliptical patch ultra-wideband antenna fed by a transmission line for the near-field characterization of cancerous cells in the skin. The antenna comprises an elliptical patch, stub loading to shift the band to lower bands, and an electronic bandgap structure on the ground side. Even though the antenna has a low profile of $15 \times 15\,mm^2$, the proposed antenna has more promising results than recent studies. Furthermore, both simulated near-field and far-field results show a broad bandwidth of 3.9–30 GHz and a resonance at 2.4 GHz applicable for industrial, scientific, and medical band applications. The proposed antenna also illustrates a peak gain of 6.48 dBi and a peak directivity of 7.09 dBi. Free space and skin (on a layer of breast fat and a tumor with a diameter of 4 mm at the boundary of skin and breast) are used as test environments during the simulation and measurement of near-field and far-field investigations while considering a phantom breast shape. Both far-field and near-field microwave investigations are performed in Computer Simulation Technology studio, and results are then compared with the measured data. The simulated and measured results are in good agreement, and the focused energy around the tumor is completely reconstructed. Therefore, the proposed antenna can be an adequate candidate for the differentiation of breast skin and tumor to reconstruct the tumor's image.

I. INTRODUCTION

Skin cancer is one of the most prevalent cancers throughout the world due to its high chance of occurrence upon body exposure to the sunlight. The human body is exposed to sunlight during the day, and sometimes, it absorbs too much UV that could harm skin cells when they are exposed for a long time. Imaging systems have many applications, such as in localization and identifying concealed threats such as weapons in airports (i.e., security and surveillance) and non-destructive testing for medical purposes.[1–6] One of the most interesting fields of studies yet to explore is the development of an ultra-wideband (UWB) imaging system for biomedical applications, such as imaging of the human tissue.[7,8]

Ultra-wideband (UWB) technology uses wide bandwidth (BW) and low power that render it suitable for low-range data communication with high rate and radar communications. Furthermore, UWB systems provide a wide BW to attain high-resolution images while imaging and detecting malignant tissue cells. The UWB technology is characterized by non-ionizing impact, low cost, and penetration capabilities, indicating its potential imaging applications.

Many methods such as magnetic resonance imaging (MRI), ultrasound, and x rays are used in clinics (using dermoscopy images and skin melanoma image evaluations) and hospitals to obtain a tomographic image of living tissues. However, these techniques have many disadvantages, including low image contrast and long scanning period.[9–11]

Generally, skin cancer is categorized as basal cell carcinoma, squamous cell carcinoma (SCC), and melanoma. They can all be detected in the early stages. Thus, the dielectric properties of the skin are helpful parameters for obtaining more accurate skin images. Furthermore, the microwave (MW) imaging technique can differentiate two materials with two different dielectric constants. The human skin as a medium under test contains three layers, namely, the epidermis, the dermis, and the hypodermis. Their thicknesses range from 0.1 to 0.5 mm.[12]

Skin cancer requires shorter wavelengths as compared to the other parts of the human body, such as the lungs, kidney, and breast. Several studies have been performed using millimeter waves (mm-wave) and terahertz (THz) waves for skin cancer imaging. On the other hand, most MW imaging systems for medical applications, especially cancer diagnosis, use longer wavelengths in the range of 300 MHz–10 GHz, whereas others use a shorter wavelength associated within the frequency range of 30–300 GHz. In addition to that, the applicable wavelength to the body is in a regime between 0.6 and 1.2 mm.[13] These wavelengths render them highly effective in any change in each layer of the skin. These layers have a high chance of being attacked by cancerous cells.[13]

Despite all the advantages of mm-wave antennas in imaging applications, especially imaging of skin and the significant contrasts between dielectric properties of normal skin, the limitations of the current mm-wave systems on BW still exist. Besides, utilizing a higher frequency band requires more complicated structures and shows availability difficulties. Furthermore, the current millimeter-wave imaging systems were realized to present limited axial resolution.[7] The pathological changes in different layers of skins, the place where the tumors generate, require a high resolution to differentiate and wide BW accordingly. Therefore, a UWB system in the microwave frequency regime is required to both cover the UWB band based on the Federal Communications Commission (FCC) and operate at higher bands close to the mm-wave range because obtaining wider BW is essential in high accuracy imaging. It will be informative to discuss the usage possibility of the type of current materials used as both antennas' substrate and conductor in antenna design technologies.

Use of electronic devices vulnerable to wear has been affected by the types of the materials that were used as the substrate and/or conductor. To incorporate electronic devices such antennas onto the human body, which is normally related to curvilinear surfaces and dynamically changing movements, the bio-integrated instruments should be physically flexible or even stretchable. As a vital element of wireless technology, a typical patch antenna that comprises a dielectric substrate and metallic resonator (conductor) in a conventional design is neither flexible nor stretchable. Since the cubic of a film thickness measures its resistance against bending deformation, reducing the thickness of a structure might be an effective way to enable flexible/bendable antennas. A stretchable Planar Inverted-F Antenna (PIFA) based on the evaporation technology has been presented. The PIFA antenna can withstand 10% strain but gives a relatively poor efficiency.[14] Stretchable, mechanically tunable, and reversibly deformable microstrip patch antennas are designed and simulated using a highly conductive and stretchable substrate. Silver nanowires suit for this purpose. The ability of stretchable antennas in applications such as wireless sensing has been approved.[15]

The recent development of flexible and stretchable antennas used for bio-integrated electronics has been concisely investigated. The current approaches incorporate application of textiles, liquid metals, graphite films, composite elastomer with conductive fillers, and structural design of conventional materials. For example, the conductive fabrics used through a weaving and knitting process showed great potential in wearable electronics technologies such as radio frequency identification tags (RFIDs). Monitoring and miniaturizing of antennas dimensions could make their mass production possible. However, the radiation efficiency of the textile antenna is disturbed when the small thickness of the metal paste is related to the condensed electrical conductivity due to the skin effect. Besides, the textile antenna related applications show limitations since the textile materials cannot be stretchable. On the other hand, applying liquid metal in polymeric microfluidic channels produces large stretchability for the antennas. For instance, a microfluidic serpentine dipole antenna indicated an adjustable sensitivity toward various geometrical designs. Both patch and ground plane superseded with meshed liquid metal channels in the microstrip antenna to detect a signal from 5 m distance. However, the liquid metal showed a low electrical conductivity, which offered a low radiation efficiency. A technique for fabricating a highly stretchable and robust antenna for radio frequency signals is presented. Liquid metals (eutectic gallium indium alloy, EGaIn) were used for these antennas as the conductor along with elastomeric microfluidic channels and silicon rubber [polydimethylsiloxane (PDMS)] as the substrate. They could be twisted and stretched up to 2.2 times of their original length.[16,17] The design concerns and challenges were succinctly examined for stretchable antennas and several reported state-of-the-art stretchable antenna designs with various fabrication tools were reviewed.[18] A stretchable antenna was recommended for body area networks operating at 2.45 GHz. The topology of the antenna was established on a meandered dipole with a parasitic arm, which had impedance with dual-resonance behavior. The prototype was applied on two stretchable technologies using thermoplastic polyurethane and silicone as substrates.[19] A 2.4 GHz unbalanced loop antenna was stretched along multiple dimensions simultaneously. It was comprehended by integrating the room temperature liquid metal alloy into microstructure channels in an elastic material.[20] A class of stretchable dipole antennas are based on embedding the three-dimensional liquid metal network into an elastically soft elastomer as conductive branches, which could be highly stretched up to a strain of 300% while presenting a high-quality reflection coefficient around −30 dB and a wide range of the tunable resonant frequency from 1.55 to 0.45 GHz simultaneously.[21] After discussing about the current possible materials used as the substrate and radiation elements of antennas especially for medical applications, the flexible/stretchable materials that are used to design UWB antennas were presented.

Many types of UWB antennas with different shapes and structures have been proposed for communication and medical purposes [health monitoring using internet of things (IoT) and wireless body

area network (WBAN)]. For instance, some studies designed a flexible UWB antenna for WBAN and IoT applications.[22–25] An UWB antenna with minimized dimensions was designed using a metal film to resonate at 7.5–10.25 GHz.[22] A flexible three-dimensional adjusted phase Vivaldi UWB antenna resonated from 6 to 18 GHz.[23] Afterward, metamaterial-based UWB antennas were investigated and designed on flexible textile substrate having miniaturized dimensions. They achieved working BW of 4.25–35 GHz and 6.5–35 GHz, respectively.[24,25] A high gain wearable metamaterial antenna was designed for skin cancer detection and resonated at a frequency band of 8–12 GHz.[26] Two more flexible UWB antennas designed for skin cancer detection and operating at the same band utilized an artificial magnetic conductor having the dimensions of 38 × 32 mm^2 and 36 × 32 mm^2, respectively.[27,28] Apart from using a flexible substrate material, several studies used a non-flexible material for the UWB antenna for both breast and skin cancer imaging.[28–33] The authors of those works tried to miniaturize the antenna that used non-flexible substrates like what was presented in Ref. 34.

It is quite challenging for UWB antennas to keep their stability in radiation characteristics and impedance performance over such a broad BW, although such a high-resolution microwave system for imaging of skin has not been introduced. A simple elliptical patch UWB antenna has a planar structure having promising characteristics such as wide bandwidth (BW) and high-gain qualities. It was designed, measured, and evaluated to be considered as one of the most suitable candidates for microwave imaging of skin[35–37] to address these issues. Elliptical patch antennas can also be easily scaled with frequency, which allows them for the realization of similarly shaped ones, resulting in an almost uniform radiation mechanism over the whole imaging bandwidth.

The present study is organized as follows: Sec. I gives a brief introduction. Section II presents the UWB imaging system and its setup. Then, the proposed antenna configurations and characterizations are discussed in Secs. III and IV, respectively. The image reconstruction procedure is detailed in Sec. V. Finally, our work is concluded in Sec. VI.

II. MICROWAVE IMAGING

Figure 1(a) shows the simulation and measurement schematic of antenna arrays. The antennas are positioned on the breast skin positioned on a breast phantom and the target. The breast phantom is chosen as a container and imaging environment to hold the antenna arrays and check the breast fat's effects on the image construction investigations of the breast skin when a malignant section exists. Besides, a space of 5 mm is considered between the antenna arrays and the skin. This space acts as a matching medium and degrades the effects of the high dielectric constant of skin in comparison with the antenna's substrate. After positioning the antenna arrays and pasting them with glue, the scattering parameters of the antenna arrays are recorded for each array antenna. These procedures are performed for multi-static imaging. It means that all the antennas send and receive signals at the same time. However, antenna 1 transmits and the others receive in our studies. All the backscattered signals are then imported to a computer for use in an image reconstruction algorithm.

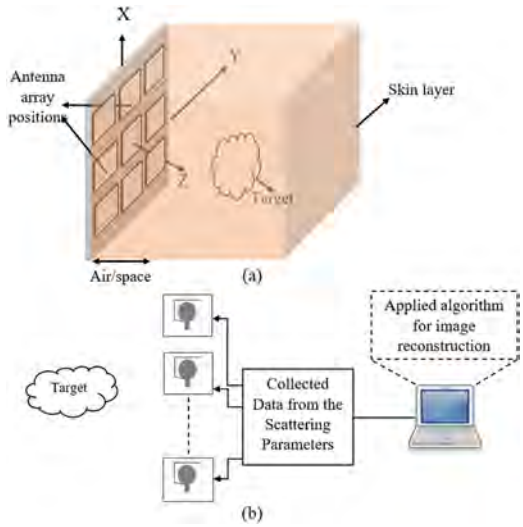

FIG. 1. Imaging-system (a) antenna arrays with skin. (b) Image reconstruction system setup.

Figure 1(b) illustrates the simulation and measurement setup of the imaging system. A performance vector analyzer (PNA; model E52466856) was used to measure the scattering parameters of the antenna arrays. The data were then imported into a computer to reconstruct the image. The antenna's ability in image reconstruction of tumor in breast skin and the required parameters only are investigated in this paper; however, the reconstructed images are added to indicate that the antenna can detect a tumor in breast and skin. The image reconstruction of the tumor is presented later.

III. ANTENNA CONFIGURATION AND OPTIMIZATION

Figures 2 and 3 illustrate the designed structure of the proposed elliptical UWB antenna. The antenna was designed on a Rogers RT/duroid 5880 layer (ε_r = 2.2 and $\tan\delta$ = 0.0009). The antenna is fed through a transmission line (TL) and then a coaxial cable accordingly. The dimensions of the patch and the TL are calculated using the equations presented in Ref. 38 to obtain the actual values of the design parameters at the desired frequency. For instance, the actual value for the TL width should be around 2.5 mm. However, it should be optimized to achieve the best outcomes. After obtaining the working BW at the center frequency of 15 GHz (the elliptical patch with the truncated ground at the back is chosen due to its simplicity, obtaining a wide BW with a simple design, ease of mounting on ordinary plastic casing, and broadside radiator with omnidirectional radiation pattern),[39] the antenna is loaded with stubs connected at the junction of the patch and the TL. It creates another resonance at the lower band and increases the ability of the antenna to work for another application [adding this stub gives the antenna the ability to work at Industrial, Scientific, and Medical (ISM) applications as well]. After adding this stub, some stop bands were created due to the mutual coupling effects and surface waves increment. A technique is required to both remove those stop bands and improve the BW. Therefore, the circular ring electronic bandgap (EBG) structure is added to compensate for the effects of

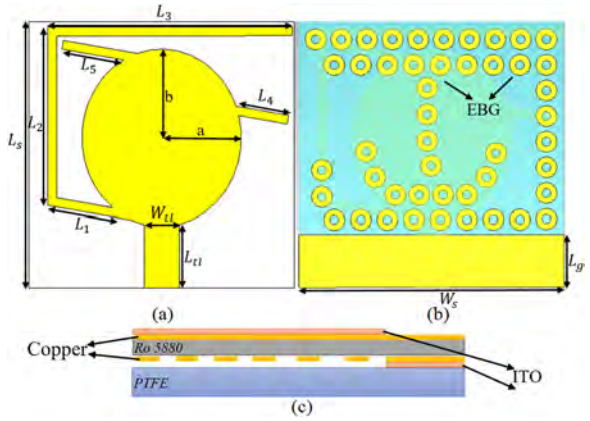

FIG. 2. Prototype of the proposed antenna [(a) front view, (b) back view, and (c) side view].

those drawbacks. These rings are located based on the surface current distribution (SCD), the fringing field around the patch, and the other part of the antenna. Both the design and optimization procedure will be explained further and in detail in the supplementary material.

In the MW imaging system, the proposed UWB antenna is used to send and receive the signals and thus detect and evaluate the skin with and without breast fat (the breast fat is used to show its existence impact on the received signals and image detection accordingly). To increase the resolution, we investigated to show how resonant frequency and BW varied in each step of the design as the broad BW and higher frequency attain higher resolution. However, frequency enhancement induced an increase in the loss of skin due to the wavelength reduction.[40]

The antenna presented in this paper sends some UWB pulses within the working BW of 3.9–30 GHz. The UWB antenna is fed through TL and SMA (SubMiniature version A) connector. A coaxial cable can deliver the UWB pulse to the SMA port and then to the TL. Thus, the TL dimension should be designed properly to avoid spurious currents and their related distortions, as well as the unwanted radiation pattern caused by the coaxial cable.[41–44] The design process started with the antenna parts, which played critical roles in preparing the ultra-wide BW, such as the patch, TL, and ground dimensions. Other parameters such as the loadings in the front and backside of the antenna with lengths of L_{1-2} and L_{4-5} did not affect the results dramatically. In addition to these loadings, a circular electronic bandgap (EBG) structure at the back formed to widen the BW of the antenna further. Besides, this EBG structure is utilized to prevent some undesired operating modes and control harmonics, also as a band-reject, especially for ultrawideband (UWB) applications. More attention is being paid to the shielding property of the EBG to reduce the specific absorption rate or SAR (back radiation). In addition, it can shield the antennas from unwanted multipath signals vital in multipoint communications.[45] The surface current distribution (SCD) shown in Fig. 5 demonstrates how the low and high end of the working BW can be achieved and varied. All dimensions were simulated and optimized using the Computer Simulation Technology (CST) studio. These dimensions are presented in terms of width and length. For instance, the length (b) and width of the patch (a) affected the lower end of the entire working BW and widened the impedance BW (a broad impedance BW was found when the impedance BW was lower than −10 dB). The ordinary elliptical UWB antenna obtained the lower end at 5.2 GHz and the first pole at 6 GHz. [Hence, we tried shifting the whole band to the lower band along with its improvement. Shifting the entire frequency band helps the antennas to work in the UWB range according to FCC (3.1–10.6 GHz). In addition, it ignores the losses that might occur at higher frequencies.] The antenna is loaded by the stub with length L_{1-3} to resonate at the ISM band and shift the entire working BW to the lower band. The length and position of this stub were selected based on the ISM-related band at 2.4 GHz and the SCD on the patch, respectively (Fig. 6). Figure 5 shows the SCD around the loaded stub and L_4 and L_5. Negative mutual coupling and surface waves were formed after adding the stubs, which were critical parameters as they degraded the radiation efficiency when the distance between the stub and patch was too short. The EBG structure is added at the back of the antenna to ignore the damaging effects of the reduced space between the stub and patch (suppress the surface waves and fringing fields).[46–49]

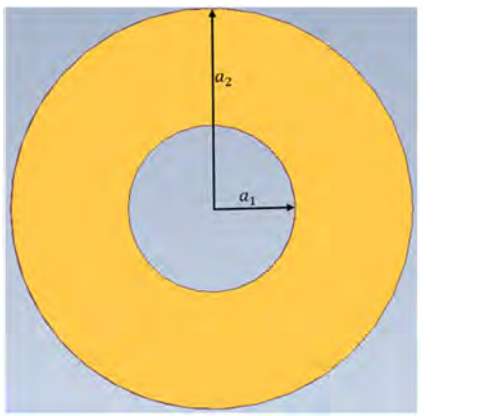

FIG. 3. EBG structure.

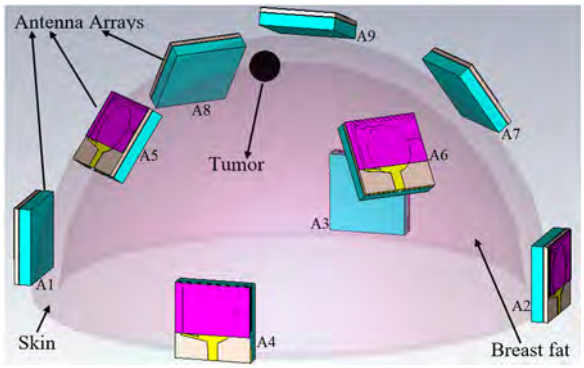

FIG. 4. Simulated array setup.[50] "Alhawari *et al.*, "Metamaterial-based wearable flexible elliptical UWB antenna for WBAN and breast imaging applications," AIP Adv. **11**, 015128 (2021). Copyright 2021 licensed under a Creative Commons Attribution (CC BY) license.

TABLE I. Antenna final dimensions.

L_s	15	L_2	10
W_s	15	L_3	13.8
a	5	L_4	3.5
b	6.75	L_5	4
L_g	3	L_{tl}	4
L_1	4	W_{tl}	5.95
a_2	0.6	a_1	0.25

Figure 4 presents the simulation setup of the system comprising a breast skin phantom with a radius of 100 mm (nearly the size of the 70A bra cup), a spherical tumor with a diameter of 4 mm (the antenna offers the BW of 26.1 GHz, and thus, it offers the range resolution of 5.7 mm; therefore, the tumor diameter was chosen to be 4 mm to examine the antenna arrays capability in detection), and nine antenna arrays. The arrays presented in Fig. 2 are located on the skin breast phantom. Generally, two parameters called clutters and artifacts affect the reconstructed image negatively and can mask the tumor response when they exist. The number of arrays can be increased to reduce the effects of these two negative parameters. Array number enhancement in the system reduced the system cost since the antenna dimensions were minimized. Based on the authors' findings, the presented antenna is the most miniaturized antenna for skin imaging in the MW regime (Table I shows the antenna dimensions).

The antenna's design parameters were optimized in free space with a permittivity of 1 when the actual dimensions of the antenna array were achieved (based on the TL equations). Afterward, the time and frequency domain characteristics were considered and investigated in free space. Besides, a layer of skin ($\varepsilon_r \cong 20$), breast fat ($\varepsilon_r = 4.7$), and tumor ($\varepsilon_r = 53.5$) underneath this space were fabricated in a 3D-printed breast phantom. The skin on the human breast and the breast phantom and fat were considered to examine their impacts on breast skin imaging.[34,51] The skin and breast fat layers are homogeneous (homogeneous in simulation and inhomogeneous breast phantom in measurement). Some design variables play important roles in improving the antenna performance based on the requirements (broad BW, stable impedance matching, and stable radiation characteristics). The parameters that affect the antenna's performance the most are as follows: the dimensions of the patch (a, b), length and width of the TL (L_f, W_f), the length of the stub (L_3), and the length of ground (L_g). CST software is used for simulation and optimization. The parameters are optimized to achieve the best result using the optimization technique of the genetic algorithm (GA) applied in CST.

The optimization procedure started with the patch dimensions and continued with the TL dimensions. The patch and TL dimensions affected the beginning and the end of the working BW. For instance, the vertical axis shifts the frequency band, and the horizontal axis enhances the BW. In addition to that, the TL's length shifts the band to either a lower or higher band (designed based on the operating frequency), and its width modifies the impedance BW to match the antenna at the operating frequency and the poles in the working BW.

The proposed antenna had six frequency poles at 5, 7.6, 10.2, 15.2, 20, and 25 GHz and one resonance at 2.4 GHz. Figure 5 presents the physical behavior of the antenna by showing the SCD

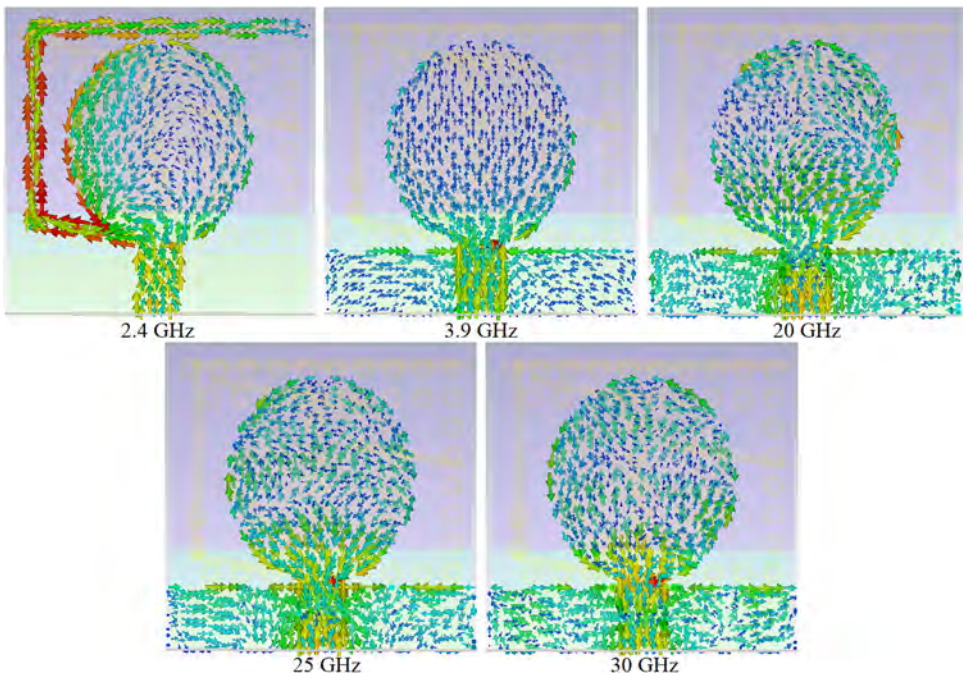

FIG. 5. Surface current distribution at 2.4, 3.9, 20, 25, and 30 GHz.

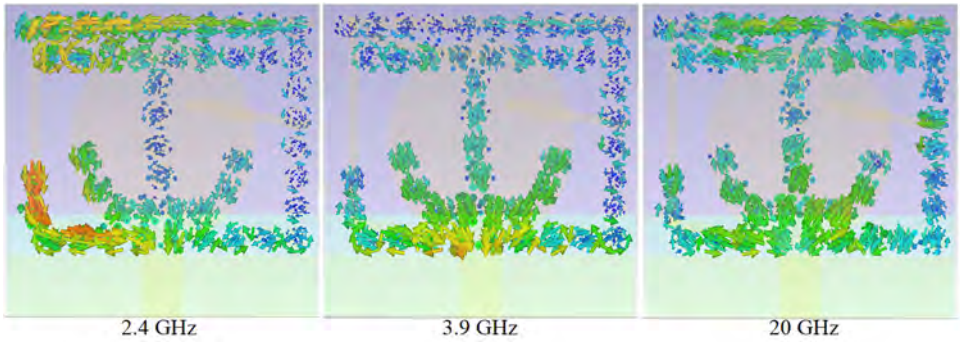

FIG. 6. Surface current distribution around the EBG structure.

at frequency bands of 2.4, 3.9, 20, 25, and 30 GHz. The UWB antennas act differently from narrowband antennas as they support the traveling-wave fundamental mode of propagation at a lower frequency band and the higher-order mode for a higher frequency band. Conversely, when the current paths on the patch and TL were changed or disturbed, the electrical characteristics of the antenna were more seriously affected based on the quarter-wave modes (Fig. 5). Moreover, the required length to resonate at 2.4 GHz is the same length as shown in Fig. 5. The SCD is significant near the edges of the stub attached to the joint point. The SCD of the antenna around the stubs, patch, stubs connected to the patch, and the TL (Fig. 5) is also more focused. Therefore, the patch and TL dimensions directly affect the lower- and higher-end of the working BW.[52,53] A layer of the polytetrafluoroethylene (PTFE) substrate with a thickness of 3.2 mm and a permittivity of 2.55 was added, after investigating the SCD around the resonator, ground, and stubs. It was considered as a cover to increase the BW and remove the stop band occurring around 24 GHz, thereby shifting the whole band to a lower frequency band (the undesired fringing fields occurred after adding this layer are compensated by the EBG structure).

Figure 6 depicts the SCD of the EBG structure added to improve the radiation efficiency of the antenna by reducing the surface waves. An intense SCD density is obtained on the EBG around the stub at 2.4 GHz. The strength of the surface current was also evident on the EBG adjacent to the transmission line and patch at the associated resonances.

Knowing how a UWB antenna works is essential. In general, the narrowband antennas propagate and operate in the frequency domain. Their parameters are assumed to be constant for some parts of their BW. Thus, for UWB antennas as impulse-based systems, the time domain characteristics are considered. Unlike the frequency domain, which is excited with a continuous wave, the time domain is excited with an impulse. The antenna's transient response (in time domain) is time-dependent and depends on the departure and angles of arrival and polarization. Figure 7 demonstrates how a pulse is sent and received in time domain.[54]

It should be mentioned that the proposed antenna is designed using a non-flexible substrate and has a miniaturized profile. Therefore, it is not necessary to use a flexible substrate and investigate the bending conditions. Besides, the proposed antenna has a low profile and is one of the smallest UWB antennas used for imaging purposes in the microwave range. Hence, it will not get too much affected by bending or dynamic changes in the skin surface.

IV. ANTENNA CHARACTERIZATION

A. Radiation characteristics of the antenna

A PNA (model E8363C) is used for measurements. The PNA is initially calibrated to increase the outcome accuracy. Then, it was

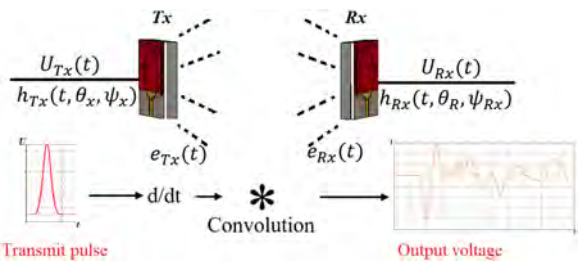

FIG. 7. Antenna system in the time domain.[55] "Saeidi *et al.* "Near-field and far-field investigation of miniaturized UWB antenna for imaging of wood," AIP Adv. **9**, 035232 (2019). Copyright 2019 licensed under a Creative Commons Attribution (CC BY) license.

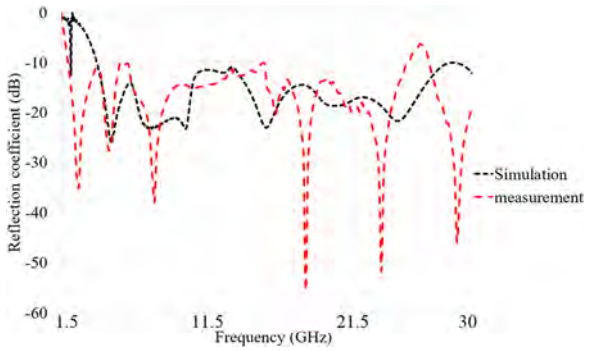

FIG. 8. Measurement and simulation results in free space.

adjusted within the frequency range of 0.5–30 GHz, and the measurement started in the air environment. Afterward, the measurement procedure uses the transmitter (Tx) and receiver (Rx) to send and receive the pulses (Tx connected to the first terminal and Rx connected to the second terminal). The Tx is kept stable at the center and the others were positioned on the other location of the skin slice based on the array's positions during the measurement, as shown in Fig. 11. The S-parameters (reflection and transmission coefficients) of each antenna array are extracted from the PNA and imported for time-domain evaluation.

Based on the simulation and measurement results shown in Fig. 8, the proposed antenna had an acceptable reflection coefficient and working BW. Figure 8 shows that the proposed antenna can be assumed as a UWB antenna because it obtained more than 26.1 GHz BW at the center frequency.

The resonance at 2.4 GHz (with a slight shift) and most of the BW 4.1–28 GHz were obtained. However, only a minor change from 3.9 GHz occurred. The reflection coefficient is less than −17 dB at most of the band, which is acceptable [voltage standing wave ratio (VSWR < 2)]. Furthermore, the optimum required BW for imaging in breast skin and air (up to 10.6 GHz) is obtained, although other researchers have used higher bands for skin imaging. The proposed antenna's BW is enhanced to have applicable antennas resonating in BW for applications such as skin-cancer imaging, which requires

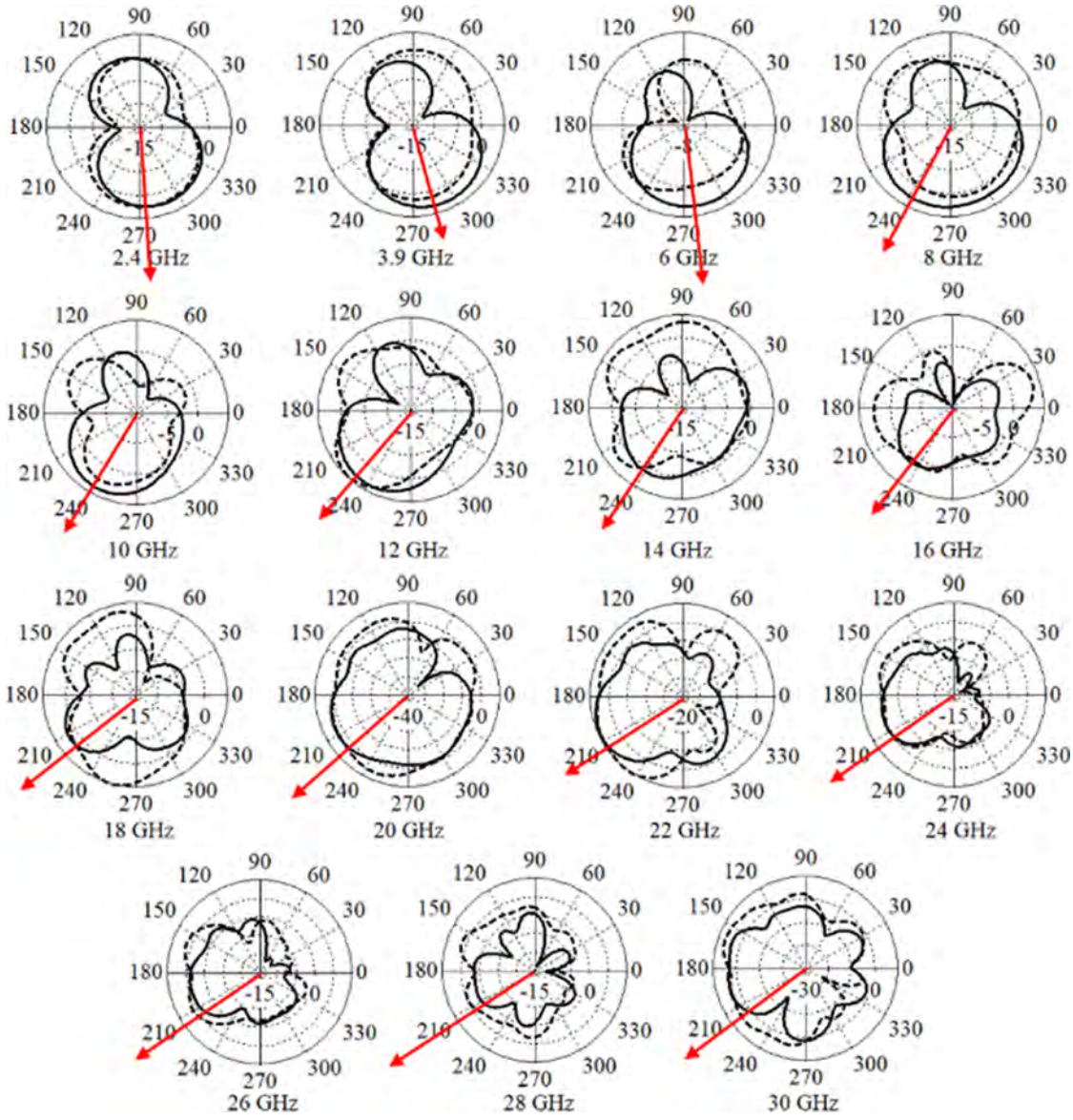

FIG. 9. Far-field radiation pattern of the proposed antenna (solid line—E-field and dashed line—H-field).

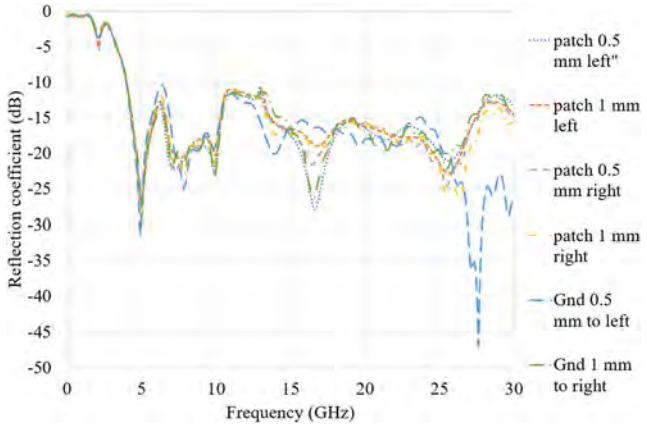

FIG. 10. S_{11} result of antenna-sensitivity analysis.

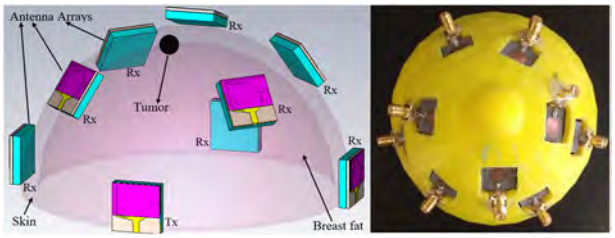

FIG. 11. Fabricated and simulated arrays and breast phantom.

lower penetration. A previous study has even applied a low THz for skin cancer.[56]

Figure 9 demonstrates the far-field radiation pattern of the antenna for E and H at $\theta = 0°$ and 90° at the working BW.[57] Given the difficulty in measuring the radiation pattern owing to the lack of equipment, only the simulation results are presented here. Besides, no standard antenna existed as a receiver that could operate in an environment with a dielectric constant of 20–47. Considering the good agreement between the simulated and measured impedance BWs, the simulated radiation pattern can be reliably performed by CST. The associated far-field gains at the working BW presented in Fig. 9 are −3.2, 0.2, 1.26, 1.8, 3.33, 3.71, 3.14, 3.06, 4.076, 5.47, 5.35, 5.734 (15 GHz), 5.76, 5.61, and 6.67 dB.

Figure 9 shows the main lobe of the radiation pattern with a red arrow, as well as the 273° main lobe at 2.4 GHz. This tendency remained without any alteration at 3.9 GHz and 6 GHz. The radiation pattern was slightly modified by almost 30°–240° at 8 GHz. Afterward, the pattern shifted to 240° and remained unchanged up to a frequency of 16 GHz . This trend is not altered at higher bands and only moved to 210° up to 30 GHz. The maximum far-field directivity and the gain of the antenna were 7.9 dBi and 6.48 dB, respectively. Moreover, the radiation efficiencies of the antenna extracted from CST through finite-difference time-domain (FDTD) analysis were 49% at 3.9 GHz, 62% at 5 GHz, 74.89% at 7 GHz, 84.8% at 9 GHz, 85.8% at 11 GHz, 84.7% at 15 GHz, 83.5% at 17 GHz, 89.4% at 20 GHz, 91.7% at 25 GHz, and 92.7% at 30 GHz.

B. Sensitivity of antenna performance to fabrication tolerances

The structure of the proposed antenna comprises stubs and gaps; accordingly, the impacts of fabrication tolerances (Fig. 10) in terms of horizontal and vertical misalignments occurring after fabrication should be investigated. Figure 10 shows the S_{11} result vs the vertical and horizontal misalignments. These tolerances are considered to avoid stop bands and mismatch points at the working BW. Figure 10 shows that misalignment did not significantly affect the matching impedance of the antenna, and only a few insignificant alterations occurred at the working BW.

C. Transmission and reflection coefficients

Figure 11 presents the simulation and measurement setup of the antenna arrays along with the array locations. The skin breast phantom is a semisphere with a diameter of 200 and a radius of 100 mm (nearly the size of a bra with a size of 70A cup). The measurement followed a similar technique performed in the simulation. Tx (A_1) sends and other arrays (A_2–A_9) arranged to receive the pulse based on Fig. 11, and then, the signal processing and investigation are started.

The transmission response (S_{21}) should be as flat as possible throughout the working BW to achieve a low distortion level in the transmitted signal from the proposed antenna to the sample.[58,59] Conversely, the S_{11} result in the breast skin environment and when the breast fat exists should not vary too much from the outcome in the air because it depicts how many waves reflected the first environment and should be less than −10 dB. The same PNA is

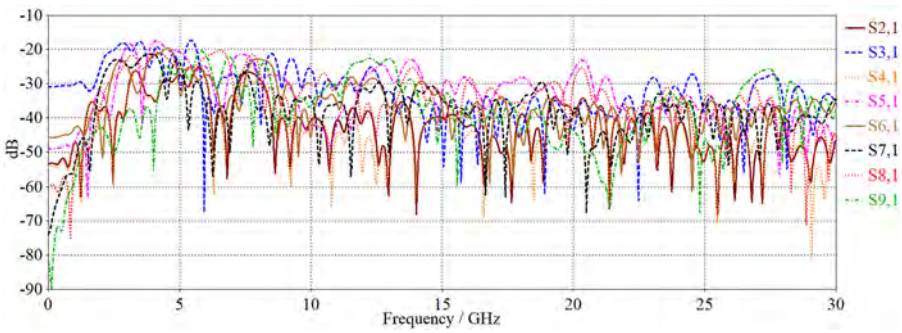

FIG. 12. Measured S21 of antenna arrays.

FIG. 13. Dielectric measurement of fabricated skin (b) and the calibration (a).

utilized to measure the reflection and transmission coefficients of the antenna. Antenna 1 is connected to the first terminal of the antenna through the cables and SMA ports. Then, the second terminal of the PNA is connected to the other arrays of the antenna. The PNA should be calibrated before performing the measurement. The calibration is started by adjusting the frequency range of 10 MHz –30 GHz. Then, the calibration kits associated with a 3.5 mm SMA port were utilized to perform the calibration. When the calibration is finished, the arrays are connected to terminal 1 and terminal 2 to carry out the measurement (A_1 is connected to terminal 1 as the transmitter and the other arrays A_2–A_9 are connected to terminal 2 as receivers). Figure 12 depicts the measured transmission-coefficient result of the array antennas around the skin and the breast phantom. Good mutual coupling and isolation were observed among the arrays because the transmission coefficient level is less than −20 dB at most of the working BW.

Figure 13 indicates the dielectric measurement of the fabricated skin. The dielectric measurement of the fabricated skin is performed to show if the fabricated skin's dielectric constant is in the presented range in the literature (~20). The probe sensor used for the measurement should be calibrated to have the best accuracy (in three stages as air, distilled water, and short section). Figure 13(a) depicts the calibration process and setup of the probe sensor. After finishing the calibration, the dielectric measurement of the fabricated skin shown in Fig. 13(b) was started. The measured relative permittivity of the fabricated skin is depicted in Fig. 14. It shows that the measured results of the relative permittivity match with the literature.[34,51]

Figure 15 illustrates the simulation result of S_{11} and S_{21} in both skins (without breast fat) and free space. An avoidable alteration of S_{11} occurred, and the entire BW shifted slightly to a higher band. The impedance BW of the antenna was marginally modified while passing the free space to reach A2. Furthermore, it resonates at 2.4 GHz, while the beginning of the BW shifts to a higher band. All alterations occurred owing to space and time delay when the signal tried to reach the receiver antenna (the increase in distance

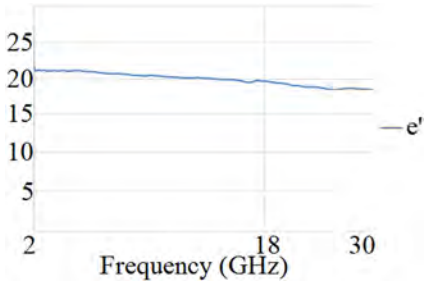

FIG. 14. Measured relative permittivity of the fabricated skin.

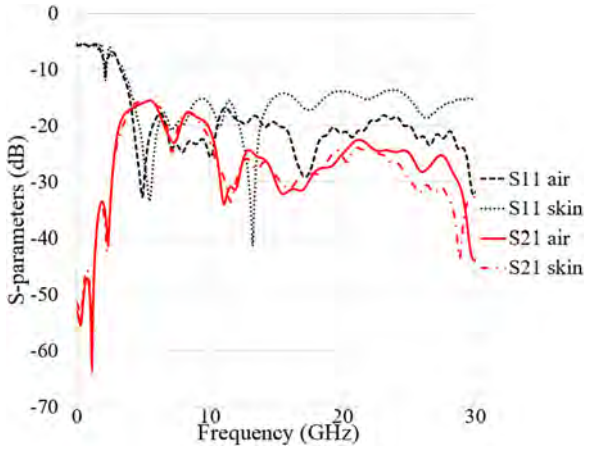

FIG. 15. Simulated reflection and transmission coefficients of the antenna in air and skin.

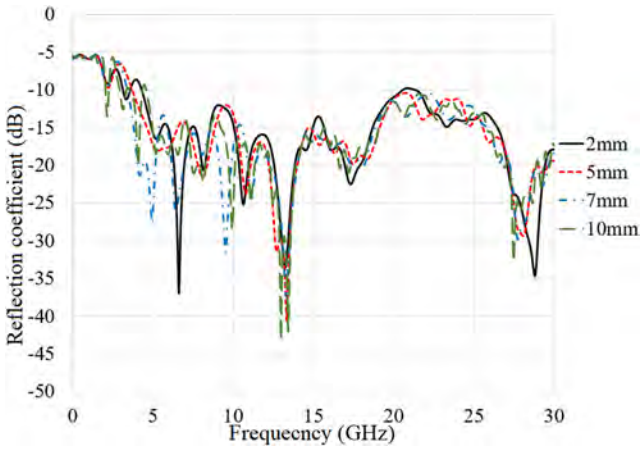

FIG. 16. Reflection-coefficient results in different thicknesses.

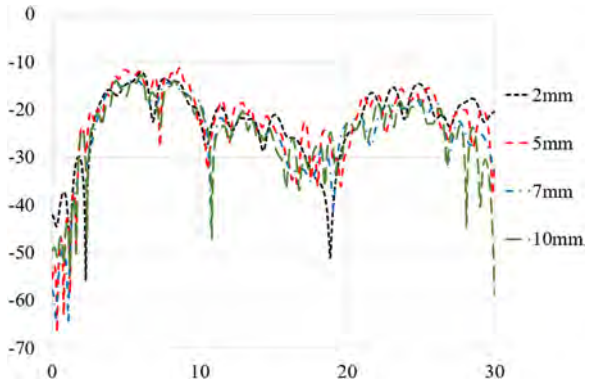

FIG. 17. Transmission-coefficient results in different thicknesses.

enhanced the time delay). Meanwhile, wave damping increased with an increase in the distance. The subjects with more height and sample with larger sizes more severely degraded the reflection-coefficient result. The impedance BW level for free space has a higher level than its outcome in skin, owing to the lower dielectric constant. The entire working BW shifted to a lower band because of the loading effect of the skin. However, the dielectric differences did not change the antenna performances. Besides, Fig. 15 shows the simulated transmission-coefficient result of the antenna in the skin and free space between two ports with 100 mm space between them. The result was better in free space than in skin for most of the working BW, except within the range of 20–23 GHz, in which the increment level was 10 dB.

As aforementioned, S_{21} should be flat to reduce the distortion in it while passing through the skin and breast fat.[46] During the measurement procedure, each antenna initially sends the pulse toward the skin sample with a total thickness of 2.5 mm (after passing the space of 5 mm), and then, the transmitted signal faced the tumor and then the breast fat (at the place of tumor). S_{21} was degraded by frequency enhancement throughout the BW. This reduction and undesired distortion were due to the reduction in wavelength at a higher frequency and the higher dielectric constant of the skin than air.

Figures 16 and 17 present the results of reflection and transmission coefficients in different thicknesses of the skin, respectively. They did not depict too much alteration when the thickness changed. Furthermore, the first resonance was still obtained when the sample changed to the skin. A significant impedance BW level was achieved too. In general, the variation in S-parameters was higher at lower conductivity.[60] When the signal faced a medium with higher conductivity, it dissipated more, resulting in increased attenuation in the reflection coefficient. The S_{21} outcomes presented applicable isolation in different thicknesses. The transmission coefficient of skin also showed a higher level for frequencies lower than 10 GHz. It was degraded after 5–30 GHz gradually and at a lower band below 5 GHz. This slight alteration may be due to the higher conductivity of the skin, which caused less penetration. In addition,

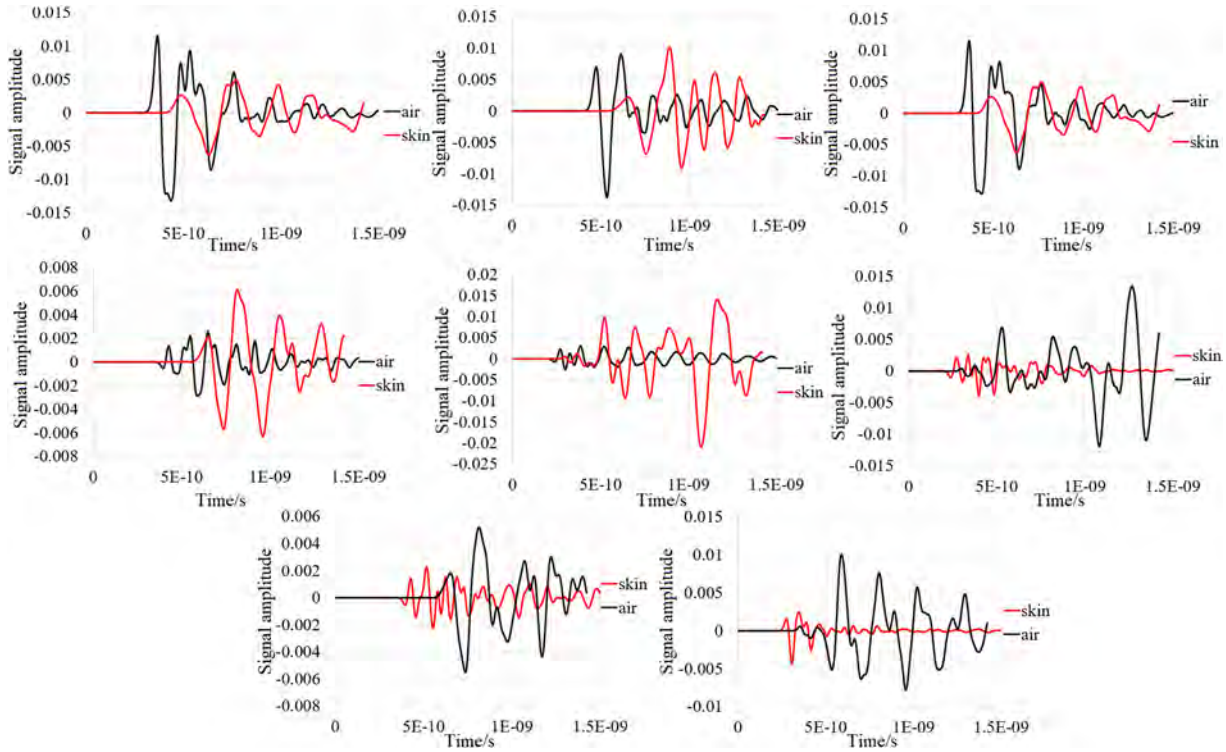

FIG. 18. Simulated received signals in skin and air.

the mutual coupling of each array in the presence of their adjacent arrays was investigated as an acceptable parameter.

The reflection-coefficient results of the arrays were not altered critically throughout the entire working BW. The slight change in the reflection coefficient indicated the loading effects due to the presence of other antenna arrays. Only two antennas were used at each measurement stage. For example, when antennas A_1 and A_5 are used, the reflection/transmission coefficients are measured. A_1 sends a UWB pulse and the other antenna (A_5) receives. This method is used because the PNA had only two ports to perform the measurement. Antenna A_1 transmitted the signal and then the other antennas received the signal presented for different arrays (A_5–A_9).

The simulated received signals in the air show the highest amplitude. When the environment changed to the skin, owing to the higher dielectric constant, the amplitude of the received signals may change and decrease. The total shape of the signal when transmitted from the Tx antenna and after passing through the environment with different dielectric constants did not change. Figure 18 shows the received signals from different angles (φ) from 0° to 180°. The shape of the signals did not change dramatically except the signal amplitude (Figs. 18 and 19). The signals' similarities and low distortion were confirmed with the fidelity percentage, as shown in Fig. 18. Hence, the proposed antenna can be an acceptable device to act as a transceiver in media such as skin and breast fat. In the simulated and measured results of the time-domain considerations, for each MW frequency, a resonant effect may have registered in the receiving antenna as an amplification of the signal in the frequency domain. This finding explained why some materials such as skin express higher transmission than others. In addition, air showed a less dielectric constant than the skin. Thus, the transmitted signal can penetrate less into the material. It should be mentioned that the measured received signals are obtained by calculating the inverse Fourier transform of the measured transmission coefficients of the antenna for each array antenna (Fig. 19).

D. Fidelity factor

The signal fidelity should be calculated when the signal distortion is a critical problem. Fidelity is considered as the magnitude of cross correlation when it reaches its maximum between the transmitted and received pulses. After achieving the received signals in the time domain from Sec. IV C, the fidelity F can be obtained, as presented in Ref. 61. The antenna's fidelity with 2.5 mm thick skin on the breast fat is depicted in Fig. 20 for different angles. One array is considered at the center (transmitter), and the others are located around the antenna at different angles to determine the fidelity factor. A pulse covering the frequency range of 3.9–30 GHz was sent from the transmitter. Based on the obtained high fidelity with a percentage of over 89% (Fig. 20), low distortion is observed in the signals. Thus, the proposed antenna can be highly recommended for use in the MW imaging of skin.[62] Besides, Fig. 20 depicts a high percentage of fidelity for both environments. The fidelity percentage is the highest for the simulated results in air, followed by the results for skin, measured in the skin, and skin with the presence of breast fat. The measured received signals are obtained by using the inverse Fourier transform of the measured transmission coefficient (S_{21}). After obtaining the measured received signals, their similarity

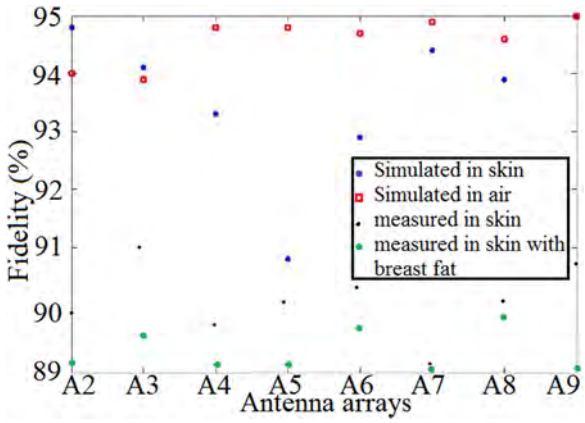

FIG. 20. Fidelity percentage of the antenna.

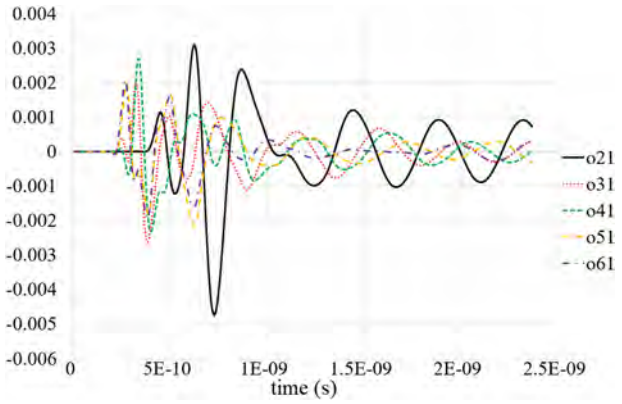

FIG. 19. Measured receive signals in skin with the presence of breast fat.

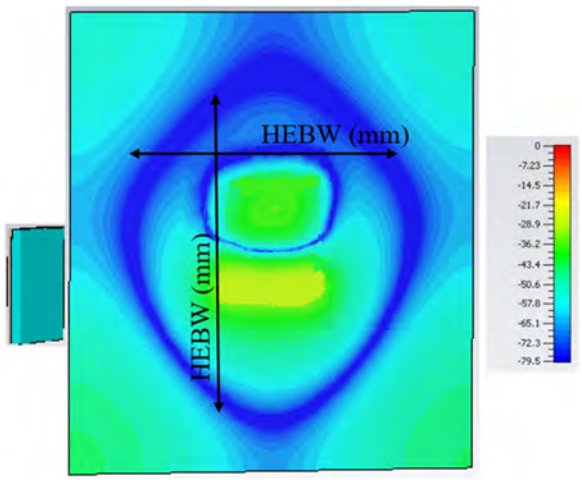

FIG. 21. Half-energy area on a plate at 12.5 GHz [HEB (X, Y, Z) in dB].

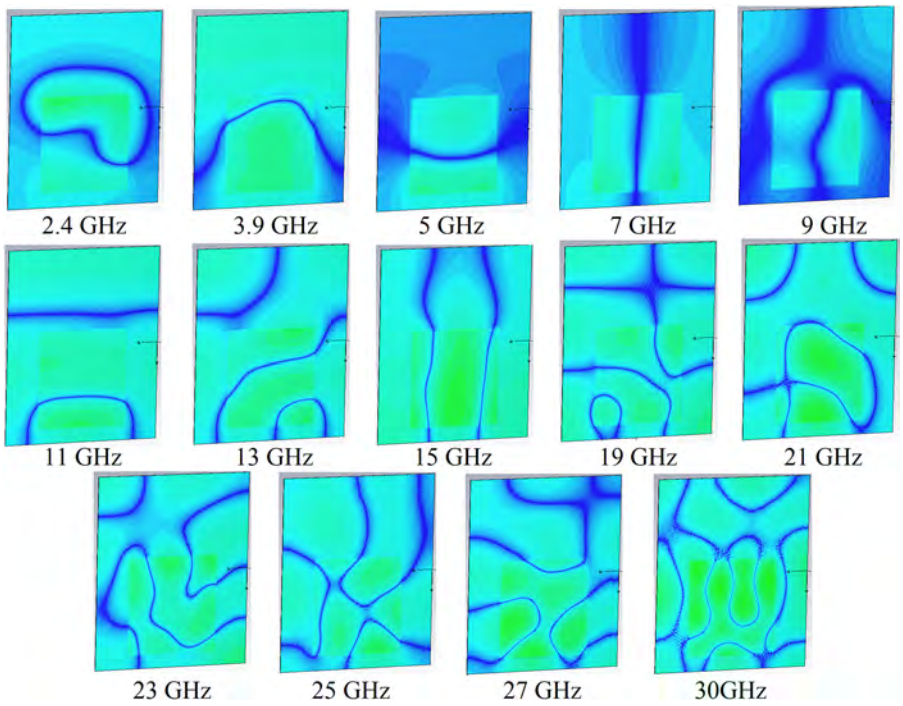

FIG. 22. EFD result at different frequencies.

percentage is investigated using the similarity index in MATLAB or using the equations in Ref. 61.

E. Near-field radiation characteristics

Two parameters are crucial in the MW field investigation of an antenna positioned at the front of a layer of skin as the half-energy beam (HEB) and the HEB width (HEBW). The energy level around the antenna itself and the skin was calculated using the pointing vector in terms of time, and the outcomes of these calculations were called the energy flux density (EFD). In addition to the EFD result, the HEBW was determined using an orthogonal plane of the skin in near-field assumptions at a certain distance. The HEBW is essential as it describes the energy that is more than half the maximum value on the same plane. Figure 21 shows the proposed antenna located in the Y direction along with the calculated HEBW in both X and Z directions. The HEBW depicts the near-field radiation beam. This near-field parameter investigation enabled us to show the antenna coverage on the desired sample. Figure 22 also illustrates the EFD result of the antenna.

Electromagnetic waves (EWs) are considered to transport data in space or through a media wirelessly. The average Poynting vector was calculated in terms of time using both electric and magnetic fields. It describes and defines the associated power and energy with these EWs. The real part of power density is average power, and it depicts how much of the power is transferred; its imaginary part showed the reactive part and how much power is stored. Figure 23 shows the real part of the Poynting vector when antenna 1 (Tx) propagated in the ZX plane for the other nine arrays. Good penetration of EWs inside the skin sample was observed (Fig. 23) and found to improve the power efficiency of the link and the ability to detect the presence of tumors in the skin.

The proposed UWB antenna is compared with recent similar existing antennas for imaging purposes, and results are shown in Table II. The antenna's performance is evaluated in terms of parameters, such as applications, 10 dB BW, dimensions, directivity, and gain. The proposed antenna may not have a higher gain than that presented in previous works. However, a good fractional BW

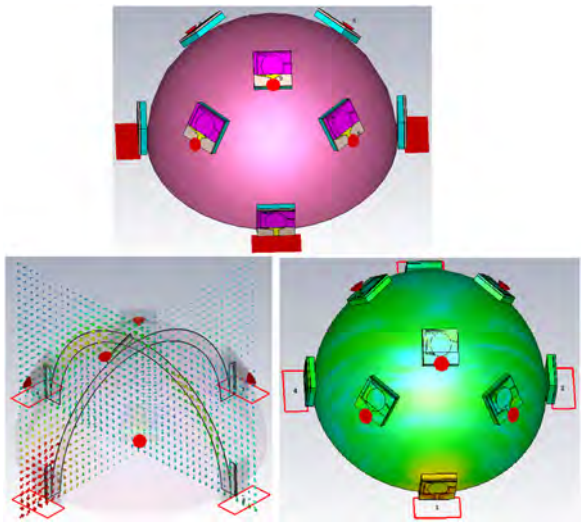

FIG. 23. Electromagnetic-wave penetration in skin.

TABLE II. Comparison between the proposed antenna and recent works (ant—antenna and application—app).

Ref	App	BW GHz (−10 dB)	Dim (mm^2)	Max directivity (dBi)/Gain (dB)
[48]	MWI	0.89–0.92,1.52–1.62,2.68–16,18.2–20	20 × 20	6.9/5.48
[61]	MWI	2.4–10	20 × 12	· · ·/3.45
[63]	UWB	3.1–10.3	60 × 60	· · ·
[64]	MWI	1.2–8.2	72 × 72	5.82/· · ·
[65]	MWI	2.68–12.06	34 × 36	6.48/· · ·
[66]	MWI	4–14	32 × 31	/6.15
[67]	UWB	3.3–12	32 × 28	· · ·/5.8
Pro	MWI	2.3–2.5, 3.9–30	15 × 15	7.9/6.49

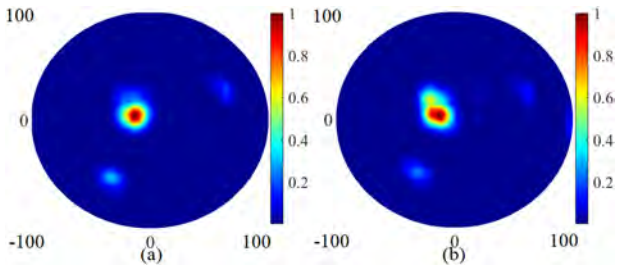

FIG. 24. Image reconstruction of image using (a) simulated and (b) measured data.

(FBW > 174%) was still achieved (f_1 = 3.9 GHz, f_2 = 30 GHz, and f_c = 15 GHz). Since the proposed UWB antenna was small, more antennas could be used for the MW imaging of skin. In comparison with recent works presented in Table II, the high performance was achieved when the antenna dimensions were minimized.

V. IMAGE RECONSTRUCTION

After showing the antennas' characteristics and proving its ability in image construction of the tumor, the received signals shown in Figs. 18 and 19 are used in the image reconstruction procedure. First, the received signal is imported in MATLAB for analysis. Afterward, the time-reversal algorithm presented in Ref. 68 is applied after importing the received signal. The energy at each point of the skin and the breast is calculated. An image that has the highest energy level as compared to the other points of the breast skin is reconstructed. Figure 24 indicates the reconstructed image of the central tumor at the boundary of the breast fat and skin presented in Fig. 11 (both simulated and measured received signals are applied to reconstruct the image). The tumor is located at X = −10 mm, Y = 5 mm, and Z = 3.5 mm (Z is the vertical distance from the breast surface).

VI. CONCLUSIONS

This paper presents a low-profile UWB antenna for the near-field microwave investigation of breast skin. The proposed antenna comprised an elliptical patch fed by a transmission line. It was loaded by short and long stubs (to resonate at 2.4 GHz and ISM band applications) connected to the patch and a circular ring EBG structure (to enhance the BW and suppress the stop bands and surface waves). The antenna had an excellent feed match at the 3.9–30 GHz frequency band (almost lower than −17 dB at most of the working BW) and 3 dB beam width of 178° in the θ = 0° and 117° in the θ = 90° plane, respectively. In addition, a maximum gain of 6.48 dB and a directivity of 7.09 dBi were achieved. The simulated and measured near-field and far-field results of the transmitted and received signals and the fields showed low distortion through air, skin, and breast fat because the antenna's fidelity was higher than 89% throughout the frequency band (3.9–30 GHz). Hence, the UWB antenna is suitable for near-field microwave characterization of breast skin, especially when the simulated and measured received signals in different environments showed good agreement. Besides, the shape of the measured signals did not change in various media. After proving the ability of the antenna arrays working in a media breast skin, both simulated and measured received signals were used to reconstruct the image of a tumor of 5 mm. The tumor was perfectly detected using both simulated and measured signals. Following the achieved results, this work supports the possibility that antennas can be adequately utilized to differentiate between the breast skin and tumor and show the focused energy at the location of the tumor in the breast skin.

SUPPLEMENTARY MATERIAL

See the supplementary material for the explanation of the main text, which contains optimization procedures of all the designed parameters such as the feed line dimensions, the patch dimensions, and the stub length.

ACKNOWLEDGMENTS

The authors acknowledge the Center for Research and Innovation Management (CRIM), UTeM's research (Grant No. JURNAL/2018/FKEKK/Q00001), and Universiti Teknikal Malaysia Melaka (UTeM) for their encouragement and help in supporting this work.

DATA AVAILABILITY

Data sharing is available with permission from UTeM University, and no further experimental data were generated at this stage of the authors' work.

REFERENCES

[1]D. M. Sheen *et al.*, "Three-dimensional millimeter-wave imaging for concealed weapon detection," IEEE Trans. Microwave Theory Tech. **49**, 1581–1592 (2001).

[2]D. M. Sheen *et al.*, "Wide-bandwidth, wide-beamwidth, high-resolution, millimeter-wave imaging for concealed weapon detection," Proc. SPIE **8715**, 871509-1–871509-11 (2013).

[3]L-3 Communications Security & Detection Systems, Inc., 2017. ProVision® Imaging, available at http://www.safeviewinc.com/advancedimaging/provision.htm.

[4]R. Appleby and R. N. Anderton, "Millimeter-wave and submillimeter-wave imaging for security and surveillance," Proc. IEEE **95**, 1683–1690 (2007).

[5]S. Shrestha *et al.*, "Microwave and millimeter wave nondestructive evaluation of the space shuttle external tank insulating foam," Mater. Eval. **63**, 339–344 (2005).

[6]M. T. Ghasr *et al.*, "Millimeter wave differential probe for nondestructive detection of corrosion precursor pitting," IEEE Trans. Instrum. Meas. **55**, 1620–1627 (2006).

[7]A. Mirbeik and N. Tavassolian, "Synthetic ultra-wideband antenna for high-resolution millimeter-wave imaging," in *IEEE International Symposium on Antennas and Propagation* (IEEE, 2015), pp. 2093–2094.

[8]A. Mirbeik and N. Tavassolian, "Ultra-high-resolution millimeter-wave imaging for biomedical applications: Feasibility study," in *Proceedings of the IEEE Biomedical Circuits and Systems Conference (BioCAS)* (IEEE, 2015), pp. 1–4.

[9]S. Shrestha, M. Agarwal, J. Reid, and K. Varahramyan, "Microstrip antennas for direct human skin placement for biomedical applications," in PIERS Proceedings, Cambridge, MA, 5–8 July 2010.

[10]Y. Guo, A. S. Ashour, and F. Smarandache, "A novel skin lesion detection approach using neutrosophic clustering and adaptive region growing in dermoscopy images," Symmetry **10**(4), 119 (2018).

[11]N. Dey, V. Rajinikanth, A. S. Ashour, and J. M. R. S. Tavares, "Social group optimization supported segmentation and evaluation of skin melanoma images," Symmetry **10**(2), 51 (2018).

[12]A. Mirbeik-Sabzevari, S. Li, E. Garay, H.-T. Nguyen, H. Wang, and N. Tavassolian, "Synthetic ultra-high-resolution millimeter-wave imaging for skin cancer detection," IEEE Trans. Biomed. Eng. **66**(1), 61–71 (2019).

[13]A. Mirbeik-Sabzevari *et al.*, "Ultra-wideband millimeter-wave dielectric characteristics of freshly-excised normal and malignant human skin tissues," IEEE Trans. Biomed. Eng. **65**, 1320 (2017).

[14]Q. Liu, K. L. Ford, R. J. Langley, and A. Robinson, S. Lacour, "Stretchable antennas," in *2012 Proceedings of the 6th European Conference on Antennas and Propagation (EuCAP)* (IEEE, 2012).

[15]L. Song, A. C. Myers, J. J. Adams, and Y. Zhu, "Stretchable and reversibly deformable radio frequency antennas based on silver nanowires," ACS Appl. Mater. Interfaces **6**, 4248–4253 (2016).

[16]J. Zhu, J. J. Fox, N. Yi, and H. Cheng, "Structural design for stretchable microstrip antennas," ACS Appl. Mater. Interfaces **11**, 8867–8877 (2019).

[17]M. Kubo, X. Li, C. Kim, M. Hashimoto, B. J. Wiley, D. Ham, and G. M. Whitesides, "Stretchable microfluidic radiofrequency antennas," Adv. Mater. **22**(25), 2749–2752 (2010).

[18]S. Jalali Mazlouman, C. Menon, R. G. Vaughan, and A. Mahanfar, "Stretchable antennas: An overview," in IEEE Antennas and Propagation Society International Symposium (APSURSI) Conference, Orlando, FL, 7–13 July 2013.

[19]A. Arriola, J. I. Sancho, S. Brebels, M. Gonzalez, and W. De Raedt, "Stretchable dipole antenna for body area networks at 2.45 GHz," IET Microwaves Antennas Propag. **5**(7), 852–859 (2011).

[20]S. Cheng, A. Rydberg, K. Hjort, and Z. Wua, "Liquid metal stretchable unbalanced loop antenna," Appl. Phys. Lett. **94**, 144103 (2009).

[21]B. Yao, X. Xu, Q. Zhang, H. Yu, H. Li, L. Ren, S. Perini, M. Lanagan, Q. Wang, and H. Wang, "Highly stretchable and mechanically tunable antennas based on three-dimensional liquid metal network," Mater. Lett. **270**, 127727 (2020).

[22]F. Iwai, T. Tanabe, S. Miyata, E. Furukawa, and H. Kanaya, "Miniaturized high-band UWB monopole metal film antenna," in 2017 IEEE International Conference on Computational Electromagnetics (ICCEM), Kumamoto, Japan, 27 April 2017.

[23]L. Sang, S. Wu, G. Liu, J. Wang, and W. Huang, "High-gain UWB vivaldi antenna loaded with reconfigurable 3-D phase adjusting unit lens," IEEE Antennas Wireless Propag. Lett. **19**(2), 322 (2020).

[24]T. Saeidi, I. Ismail, S. Nozad Mahmood, S. Alani, S. M. Ali, and A. R. H. Alhawari, "Metamatrial-based antipodal vivaldi wearable UWB antenna for IoT and 5G applications," in *2020 IEEE International Conference on Dependable, Autonomic and Secure Computing* (IEEE, 2020).

[25]T. Saeidi, S. Nozad Mahmood, S. Alani, S. M. Ali, I. Ismail, and A. R. H. Alhawari, "Sub-6G metamaterial-based flexible wearable UWB antenna for IoT and WBAN," in *2020 IEEE International Conference on Dependable, Autonomic and Secure Computing* (IEEE, 2020).

[26]Neha and A. Kaur, "Wearable antenna for skin cancer detection," in 2016 2nd International Conference on Next Generation Computing Technologies (NGCT), Dehradun, India, 14–16 October 2016.

[27]A. M. Tripathi, P. K. Rao, and R. Mishra, "An AMC inspired wearable UWB antenna for skin cancer detection," in 2020 International Conference on Electrical and Electronics Engineering (ICE3), India, 2020.

[28]A. Mersani, L. Osman, and J.-M. Ribero, "Flexible UWB AMC antenna for early stage skin cancer identification," Prog. Electromagn. Res. M **80**, 71–81 (2019).

[29]E. Porter, G. Walls, Y. Zhou, M. Popovic, and J. D. Schwartz, "A flexible broadband antenna and transmission line network for a wearable microwave breast cancer detection system," Prog. Electromagn. Res. Lett. **49**, 111–118 (2014).

[30]Y. Rahayu and I. Waruwu, "Early detection of breast cancer using ultra wideband slot antenna," SINERGI **23**(2), 115–122 (2019).

[31]S. M. Asha Banu and K. Meena Alias Jeyanthi, "An extensive survey on metamaterial based antenna design for breast cancer detection," J. Complementary Med. Res. **11**(1), 233 (2020).

[32]S. Fouad, R. Ghoname, Abd E. Elmahdy, and Abd E. Zekry, "Enhancing tumor detection in IR-UWB breast cancer system," Int. Scholarly Res. Not. **2017** 4606580.

[33]N. N. kumar, B. S. Srikanth, S. B. Gurung, S. Manu, G. N. S. Gowthami, T. Ali, and S. Pathan, "A slotted UWB monopole antenna with truncated ground plane for breast cancer detection," Alexandria Eng. J. **59**, 3767–3780 (2020).

[34]A. Mirbeik-Sabzevari, S. Li, E. Garay, H.-T. Nguyen, H. Wang, and N. Tavassolian, "Synthetic ultra-high-resolution millimeter-wave imaging for skin cancer detection," IEEE Trans. Biomed. Eng. **66**(1), 61 (2019).

[35]E. N. Tziris, P. I. Lazaridis, Z. D. Zaharis, J. P. Cosmas, K. K. Mistry, and I. A. Glover, "Optimized planar elliptical dipole antenna for UWB EMC applications," IEEE Trans. Electromagn. Compat. **61**(4), 1377 (2019).

[36]N. B. Want *et al.*, "A microstrip-fed logarithmically tapered slot antenna for wideband applications," J. Electromagn. Waves Appl. **23**, 1335–1344 (2009).

[37]V. Mikhnev and P. Vainikainen, "Wideband tapered slot antenna with corrugated edges for GPR applications," in *Proceedings of the European Microwave Conference* (IEEE, 2003), pp. 727–729.

[38]P. B. Ramesh Garg, *Microstrip Antenna Design Handbook* (Artech House Inc, 2000).

[39]M. H. Fazalul Rahiman, T. Tan Wan Kiat, S. P. Jack, and R. Abdul Rahim, "Microwave tomography application and approaches—A review," J. Teknol. **73**(3), 133–138 (2015).

[40]H. M. Jafari, M. J. Deen, S. Hranilovic, and N. K. Nikolova, "A study of ultra-wideband antennas for near-field imaging," IEEE Trans. Antennas Propag. **55**(4), 1184–1188 (2007).

[41]V. Sharma, V. K. Saxena, and K. B. Sharma, "Radiation performance of an elliptical patch antenna with three orthogonal sector slots," Rom. J. Inf. Sci. Technol. **14**(2), 123–130 (2011).

[42]S. Latif, D. Flores-Tapia, S. Pistorius, and L. Shafai, "A planar ultrawideband elliptical monopole antenna with reflector for breast microwave imaging," Microwave Opt. Technol. Lett. **56**(4), 808–813 (2014).

[43]S. Yadav *et al.*, "Design of Dual Band Sawtooth Patch Antenna Using PBG Structure," in 2015 2nd International Conference on Signal Processing and Integrated Networks (SPIN, 2015).

[44]N. Mohammedi, S. Zaiter, and R. Oussaid, "Theoretical study of PBG materials as substrates to enhance antenna performance," in *2014 International Conference on Multimedia Computing and Systems (ICMCS)* (IEEE, 2014), pp. 4799–3824.

[45]Md. Shahidul Alam, N. Misran, B. Yatim, and M. Tariqul Islam, "Development of electromagnetic band gap structures in the perspective of microstrip antenna design," Int. J. Antennas Propag. **2013**, 507158.
[46]A. I. Imran and T. A. Elwi, "A cylindrical wideband slotted patch antenna loaded with frequency selective surface for MRI applications," Eng. Sci. Technol., Int. J. **20**, 990–996 (2017).
[47]R. Kumar and A. Saxena, "Elliptical micro-strip patch antenna for circular polarization design using HFSS," Int. J. Eng. Technol. Res. **3**, 1408–1411 (2016).
[48]P. C. Sharma, T. K. Bandopadhyay, and P. Tilanthe, "A compact UWB antenna with dual band," Prog. Electromagn. Res. B **35**, 389–405 (2011).
[49]K. Raj, S. Rajoriya, and P. K. Singhal, "Monopole antenna with modify ground plane," Int. J. Eng. Technol. **1**(3), 266–270 (2012).
[50]A. R. H. Alhawari, A. H. M. Almawgani, A. T. Hindi, H. Alghamdi, and T. Saeidi, "Metamaterial-based wearable flexible elliptical UWB antenna for WBAN and breast imaging applications," AIP Adv. **11**, 015128 (2021).
[51]A. Mashal, F. Gao, and S. C. Hagness, "Heterogeneous anthropomorphic phantoms with realistic dielectric properties for microwave breast imaging experiments," Microwave Opt. Technol. Lett. **53**(8), 1896–1902 (2011).
[52]T. Saeidi, I. Ismail, W. P. Wen, A. R. H. Alhawari, and A. Mohammadi, "Ultra-wideband antennas for wireless communication applications," Int. J. Antennas Propag. **2019**, 7918765.
[53]P. Moeikham, C. Mahatthanajatuphat, and P. Akkaraekthalin, "A compact UWB antenna with a quarter-wavelength strip in a rectangular slot for 5.5 GHz band notch," Int. J. Antennas Propag. **2013**, 574128.
[54]A. Shlivinski, E. Heyman, and R. Kastner, "Antenna characterization in the time domain," IEEE Trans. Antennas Propag. **45**(7), 1140–1149 (1997).
[55]T. Saeidi, I. Ismail, A. R. H. Alhawari, and W. P. Wen, "Near-field and far-field investigation of miniaturized UWB antenna for imaging of wood," AIP Adv. **9**, 035232 (2019).
[56]D. Xu, Z. Wang, Y. Wang, and J. Wu, "A high performance ultra-wideband low cost SMA-to-GCPW transition," IEICE Electron. Express **13**(12), 20160290 (2016).
[57]K. Mitsuhashi, K. Wang, and M. A. Anastasio, "Investigation of the far-field approximation for modeling a transducer's spatial impulse response in photoacoustic computed tomography," Photoacoustics **2**, 21 (2013).
[58]D. Lamensdorf and L. Susman, "Baseband-pulse-antenna techniques," IEEE Antennas Propag. Mag. **36**(1), 20–30 (1994).
[59]H. I. Hraga, C. H. See, R. A. Abd-Alhameed, S. M. R. Jones, M. B. Child, I. T. E. Elfergani, and P. S. Excell, "Design of a planar inverted F-L antenna (PIFLA) for lower-band UWB applications," in *Proceedings of the Loughborough Antennas & Propagation Conference (LAPC)* (IEEE, Loughborough, UK, 2010), pp. 485–488.
[60]P. F. Medina, A. Lucibello, G. Granse, E. Brinciotti, M. Kasper, A. O. Oladipo, R. Feger, A. Stelzer, H. Tanbakuchi, R. Stancliff, E. Proietti, R. Marcelli, and F. Kienberger, "Transmission and reflection mode scanning microwave microscopy (SMM): Experiments, calibration, and simulations," in *Proceedings of the 45th European Microwave Conference* (IEEE, 2015).
[61]T. A. Elwi, "Novel UWB printed metamaterial microstrip antenna based organic substrates for RF-energy harvesting applications," AEU - Int. J. Electron. Commun. **101**, 44 (2019).
[62]M. Islam, M. T. Islam, M. R. I. Faruque, M. Samsuzzaman, N. Misran, and H. Arshad, "Microwave imaging sensor using compact metamaterial UWB antenna with a high correlation factor," Materials **8**, 4631–4651 (2015).
[63]M. N. Shakib, M. Moghavvemi, and W. N. L. Mahadi, "A low-profile patch antenna for ultrawideband application," IEEE Antennas Wireless Propag. Lett. **14**, 1790–1793 (2015).
[64]R. Yahya, M. R. Kamarudin, N. Seman, M. I. Sabran, and M. F. Jamlos, "Investigation on CPW koch antenna durability for microwave imaging," in *PIERS Proceedings* (PIERS, Taipei, 2013), pp. 498–501.
[65]R. Karli, H. Ammor, and J. E. Aoufi, "Miniaturized UWB microstrip antenna for microwave imaging," WSEAS Trans. Inf. Appl. **11**, 122–129 (2014).
[66]R. Kumar and P. N. Chaubey, "On the design of tree-type ultra-wideband fractal antenna for DS-CDMA system," J. Microwaves, Optoelectron. Electromagn. Appl. **11**(1), 107–121 (2012).
[67]Y. L. Dai, B. Yuan, X. H. Zhang, X. W. Dai, and G. Q. Luo, "A novel compact ultra-wideband metamaterial-based microstrip," in *2016 IEEE MTT-S International Microwave Workshop Series on Advanced Materials and Processes for RF and THz Applications (IMWS-AMP)* (IEEE, 2017), Vol. 16, pp. 4–6.
[68]S. Mukherjee, L. Udpa, S. Udpa, and E. J. Rothwell, "Target localization using microwave time-reversal mirror in reflection mode," IEEE Trans. Antennas Propag. **65**(2), 820–828 (2017).